International Journal of Hydrogen Energy 124 (2025) 345–354

Contents lists available at ScienceDirect

International Journal of Hydrogen Energy

journal homepage: www.elsevier.com/locate/he

Electrochemical oxidation of guaiacol as a sacrificial anodic process producing fine chemical derivative, for hydrogen production via electrolysis

Andrea Severini [a,1], Camilla Ferrari [b,1], Andrea Marchetti [a,e,*], Francesco Vizza [c], Marco Bonechi [d,e], Massimo Innocenti [d,e], Valeria Lagostina [f], Enrico Salvadori [f], Mario Chiesa [f], Fabrizio Roncaglia [a,e,g,**], Claudio Fontanesi [b,e,***]

[a] Department of Chemical and Geological Sciences, (DSCG), University of Modena and Reggio Emilia, Via Giuseppe Campi 103, 41125, Modena, (MO), Italy
[b] Department of Engineering "Enzo Ferrari", (DIEF), University of Modena and Reggio Emilia, Via Vivarelli 10, 41125, Modena, Italy
[c] Italian National Research Council (CNR), Institute of Chemistry of OrganoMetallic Compounds (ICCOM), Via Madonna Del Piano 10, Sesto Fiorentino, 50019, Florence, Italy
[d] Department of Chemistry, "Ugo Schiff", University of Firenze, via della Lastruccia 3, 50019, Sesto Fiorentino, Italy
[e] National Interuniversity Consortium of Materials Science and Technology (INSTM), Via G. Giusti 9, 50121, Firenze, (FI), Italy
[f] Department of Chemistry, University of Torino, Via Giuria 7, Torino, 10125, Italy
[g] Interdepartmental Centre H2-MORE, University of Modena and Reggio Emilia, Via Università 4, 41125, Modena, Italy

ARTICLE INFO

Keywords:
Hydrogen evolution reaction
Guaiacol
Sacrificial oxidation
Mechanism
Fine chemicals by-product

ABSTRACT

In this paper we propose an alternative strategy to produce *green hydrogen* in a more sustainable way than standard water electrolysis, where a substantial amount of the electrical energy is wasted in the oxygen evolution quite often simply released in the atmosphere. The HER (hydrogen evolution reaction) is effectively coupled with the oxidation of guaiacol at the anode, leading to the simultaneous production of H_2 and valuable guaiacol oligomers. Significative points **i)** a substantial decrease of the potential difference for the HER, 0.85 V with guaiacol **ii)** HER is accompanied by the production of industrially appealing and sustainable guaiacol based oligomers **iii)** guaiacol oxidation runs efficiently on carbon-based surfaces like graphite and glassy carbon, which are cheap and not-strategic materials. Then, the electrochemical oxidation mechanism of guaiacol is studied in detail with *in-situ* EPR measurements and post-electrolysis product characterization: LC-DAD, LC-MS and NMR. Experimental results and theoretical calculations suggest that guaiacol polymerization follows a Kane-Maguire mechanism.

1. Introduction

Green hydrogen is gaining more and more attention as the ideal energy carrier, since it can be produced via water electrolysis and yields water as the combustion product [1].Because of that, the use of hydrogen as a fuel or energy vector is considered a key strategy for a decarbonized energy infrastructure. Furthermore, the increasing availability of efficient renewable photovoltaic and wind (electric) energy industrial installations will make *green hydrogen* production even cleaner and cheaper in the next future. The challenge *green hydrogen* is facing today lies in the cost of the high energy requirement for the electrochemical water splitting. The conventional water electrolysis process involves two half-reactions: oxidation at the positive electrode (anode) with oxygen evolution (OER) and reduction at the negative electrode (cathode) with hydrogen production (HER). Useful levels of H_2 production via conventional water electrolysis can only be achieved with an

* Corresponding author. Department of Chemical and Geological Sciences, (DSCG), University of Modena and Reggio Emilia, Via Giuseppe Campi 103, 41125, Modena, (MO), Italy.
** Corresponding author. Department of Chemical and Geological Sciences, (DSCG), University of Modena and Reggio Emilia, Via Giuseppe Campi 103, 41125, Modena, (MO), Italy.
*** Corresponding author. Department of Engineering "Enzo Ferrari", (DIEF), University of Modena and Reggio Emilia, Via Vivarelli 10, 41125, Modena, Italy.
E-mail addresses: andrea.marchetti@unimore.it (A. Marchetti), fabrizio.roncaglia@unimore.it (F. Roncaglia), claudio.fontanesi@unimore.it (C. Fontanesi).
[1] Authors Andrea Severini and Camilla Ferrari contributed equally.

https://doi.org/10.1016/j.ijhydene.2025.03.439
Received 6 December 2024; Received in revised form 26 February 2025; Accepted 30 March 2025
Available online 8 April 2025

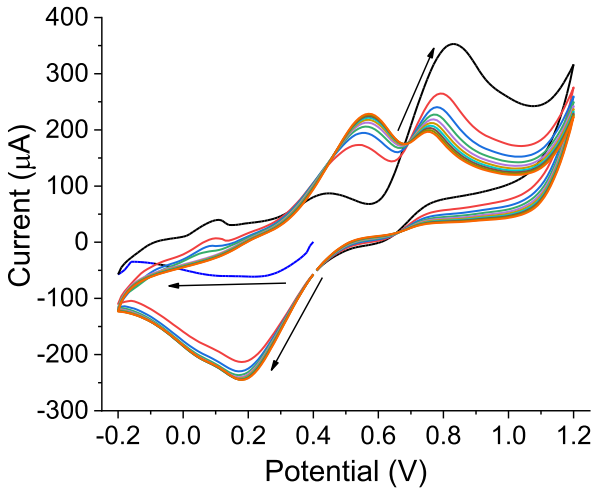

Fig. 1. CV curves of an aqueous solution of guaiacol 0.5 mM, TFA 1 mM and KCl 10 mM, recorded in the −0.2 to +1.2 V potential range, at a potential scan rate of 100 mV/s, starting from +0.4 V (OCP). Glassy carbon as working electrode, Pt wire as counter electrode, Ag/AgCl KCl_{sat} as reference electrode. The arrow indicates the start and the direction of the CV scans.

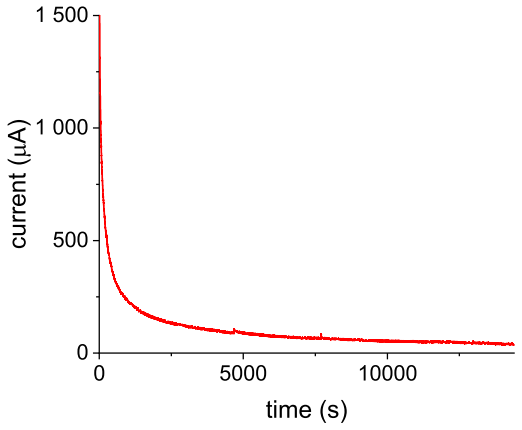

Fig. 2. 4 h chronoamperometry at +0.8V of an aqueous solution of guaiacol 10 mM, TFA 20 mM, KCl 0.2 M. Graphite lead as working electrode, Pt wire as counter electrode, Ag/AgCl KCl_{sat} as reference electrode.

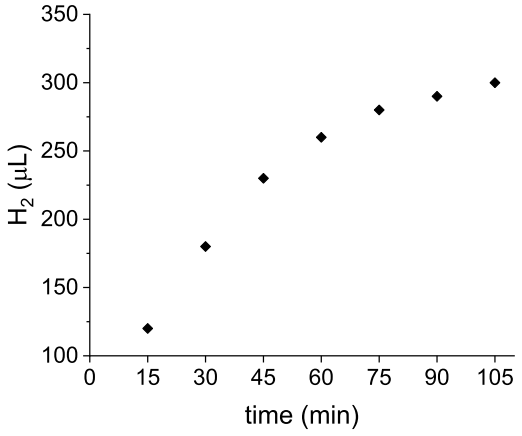

Fig. 3. The volume of hydrogen produced during electrolysis of an aqueous solution of guaiacol as a function of time. Guaiacol 10 mM, TFA 20 mM, KCl 0.2 M at +0.8 V for 105 min. Graphite lead as working electrode, Pt wire as counter electrode, Ag/AgCl/KCl_{sat} as reference electrode.

electrical energy input greater than 45 kWh/kg H_2 [2] and approximately 15 kg water/kg H_2 [3]. For this reason, research efforts are still needed to improve the energy efficiency of electrolyzers. Some not-conventional solutions, such as the thermal activation of the electrolytic process [4], or exploiting spin control [5–9] have been proposed. However, heating leads again to a significant increase in energy costs. Furthermore, in water electrolysis the desired product (H_2) is produced at the cathode, while gaseous oxygen is generated at the anode [2]. Although pure O_2 is used in various industrial applications and has some economic value, oxygen harvesting and storage require plant sophistication and a corresponding capital investment. As a consequence, oxygen is often simply released into the atmosphere. Thus, the lower utility of the anodic process, combined with the intrinsic energy requirement for the OER, calls for a different strategy to make the anodic process productive and profitable. This can be achieved by coupling hydrogen reduction at the cathode with oxidative processes that yield valuable chemicals. In this work we propose to couple HER with guaiacol oxidation as a sacrificial anodic process. Guaiacol is a non-toxic *o*-methoxyphenol derived from guaiacum or lignin pyrolysis. Due to its properties it finds industrial application across various sectors [10]. For example, it serves as a precursor for guaifenesin in cough syrups, it possesses antiseptic and local anesthetic properties, and it is used as a flavoring agent, either directly or after modification such as in the synthesis of vanillin [11]. The present study is based on a seminal paper by Papouchado on the guaiacol electrochemical oxidation, where the reported onset potential for guaiacol oxidation is found much lower than the thermodynamic OER onset potential needed for water splitting (+1.23 V [2]). Moreover, the formation of para-coupled guaiacol oligomers was suggested to be the main product following guaiacol oxidative coupling [12]. In this paper the HER efficiency is analysed in tight comparison to an in-depth characterization of the oxidation products. The guaiacol oligomer production is suggested to follow a Kane−Maguire mechanism [13–18]. The evolved hydrogen gas volume is also collected as a function of time to determine the process dynamics and faradic efficiency.

2. Experimental

2.1. Chemicals

Reagent grade potassium chloride (KCl, ≥ 99.5 %), phosphoric acid (H_3PO_4, 85 %) and sodium bicarbonate ($NaHCO_3$) were purchased from Carlo Erba Reagents. Food grade guaiacol (≥99 %), dichloromethane (DCM, 99.9 %), tetrabutylammonium hexafluorophosphate (TBAHFP, 98 %), perchloric acid ($HClO_4$, 60 %) and deuterated chloroform ($CDCl_3$) were purchased from Sigma Aldrich. Sulfuric acid (H_2SO_4, 96 %) was purchased from J. T. Baker. Trifluoroacetic acid (TFA, ≥ 98.0 %) was purchased from Fluka. Magnesium sulphate ($MgSO_4$, 99.5 %) was purchased from Alfa Aesar. Biosolve HPLC-S grade, acetonitrile (MeCN) was used to prepare eluent solutions for HPLC analysis. All chemicals were used without further purification.

2.2. Electrochemical experiments

Electrochemical experiments were conducted with a PalmSens4™ potentiostat, typical three electrodes measurements were carried out in a cell equipped with a glassy carbon rod (GC, diameter = 1.96 mm, length = 2.5 cm) or a graphite lead as the working electrode (WE, diameter = 1.93 mm, length = 13 cm), a Pt wire as the counter electrode (CE, diameter = 0.50 mm, length = 8 cm) and a Ag/AgCl/KCl_{sat} electrode as the reference electrode (RE). For EPR measurements two Pt wires were used as both the WE and the CE. The software used to operate the potentiostat, record and process data was PSTrace 5.9. The efficiency of different electrode materials was probed in screening experiments: several cyclic voltammetry and chronoamperometry were carried out using different electrode materials. Pt, Au, GC and graphite were all

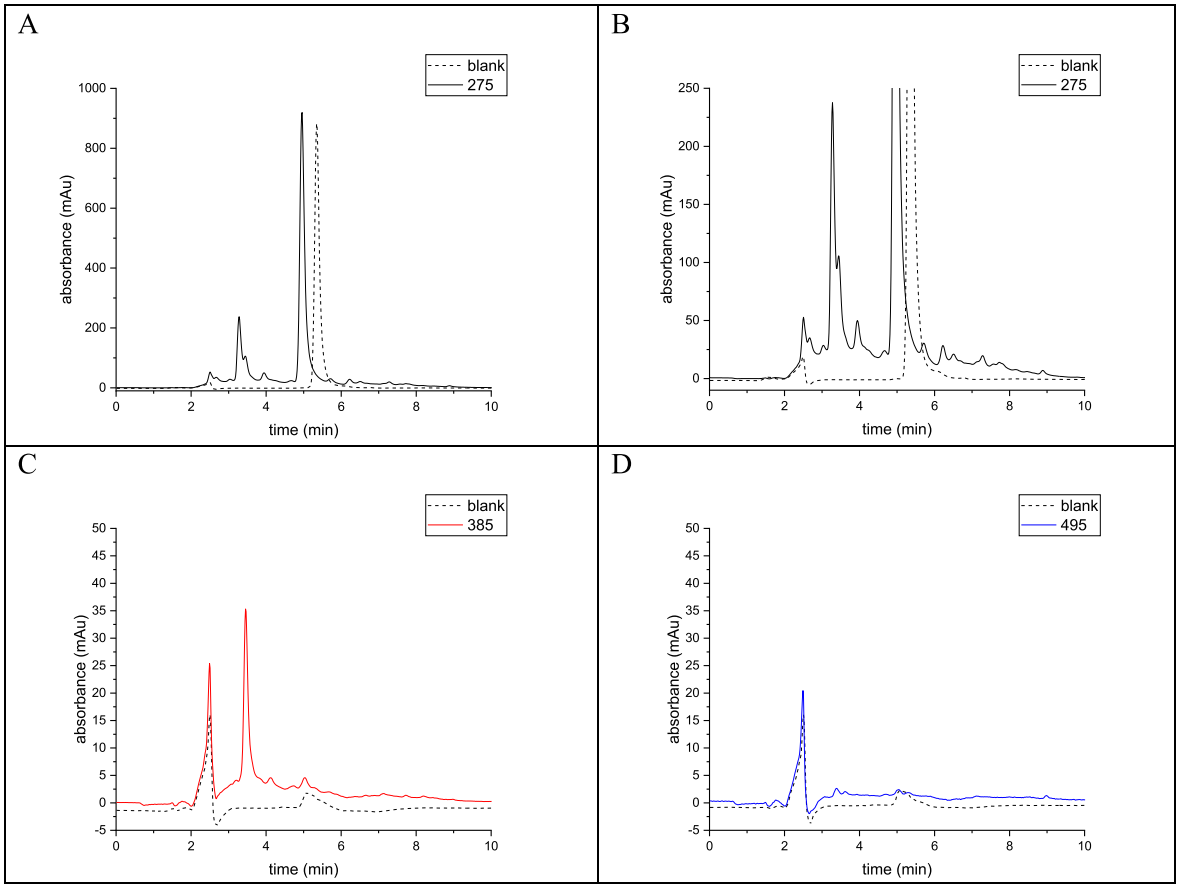

Fig. 4. Chromatograms of a 20-fold diluted sample of an aqueous solution of guaiacol 10 mM, TFA 20 mM and KCl 0.2 M, before (dashed line) and after (solid line) 4 h of constant potential electrolysis at +0.8V. A) chromatogram recorded at 275 nm, B) magnification of A, C) chromatogram recorded at 385 nm, D) chromatogram recorded at 495 nm.

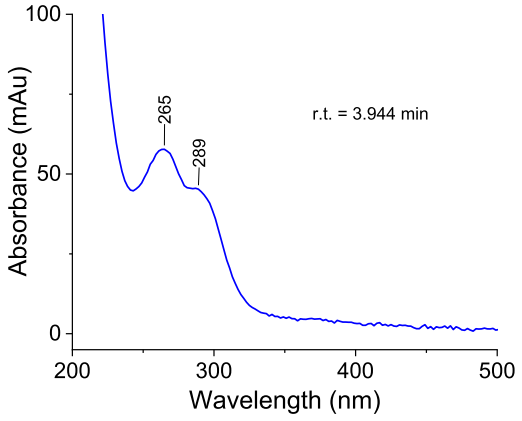

Fig. 5. UV–Vis spectrum of the molecule featuring a retention time (r.t.) of 3.944 min.

tested as WE for the oxidation of guaiacol. Among these, graphite performed the best, meaning that higher currents were measured at the same voltages. Similarly, Pt and GC counter electrodes were compared too. GC in particular was characterized by a substantial decrease in efficiency, i.e. lower current values. Thus, the best performing couple of electrodes for electrolysis was found to be graphite as WE (OER) and Pt (HER) as the CE.

2.2.1. Bulk electrolysis

For bulk electrolysis measurements 2 mL of an aqueous solution of guaiacol (10 mM), TFA (20 mM) and KCl (0.2 M) were electrolyzed for 4 h at constant +0.8 V. To maximize the electrode's surface-to-volume ratio, the solution was poured into a flame-sealed Pasteur pipette, and the graphite lead electrode was used as the WE. A Pt wire and an Ag/AgCl/KCl_{sat} were used as CE and RE respectively.

2.2.2. Hydrogen co-production

Measurement of hydrogen co-production: 8 mL of an aqueous solution of guaiacol (10 mM), TFA (20 mM) and KCl (0.2 M) were electrolyzed for 105 min at constant +0.8 V. A graphite working electrode was used as the WE, a Pt wire as the CE, and the potential applied was monitored using an Ag/AgCl/KCl_{sat} RE. The volume of hydrogen gas produced at the CE during electrolysis was measured by embedding the Pt wire in a flame-sealed graduated pipette. The pipette was filled with the guaiacol solution during the experimental setup, then the displacement of liquid due to gas evolution was recorded within 15 min time intervals.

2.3. UV–vis and UV–vis spectroelectrochemistry

UV–Visible spectra of the oxidized guaiacol solution were recorded using a PerkinElmer Lambda 650 UV–Vis spectrometer in the spectral range 800 ÷ 200 nm using a dual-beam configuration and 1 cm quartz cuvettes. The first stages of the electrolysis were monitored via UV–Vis spectroelectrochemistry. The electrolysis was performed in the quartz cuvette using a graphite lead as the WE, a Pt wire as the CE and an Ag/AgCl/KCl_{sat} as the RE. Oxidation potential was set at +0.8 V, and the UV–Vis spectrum of the solution was recorded at each 1-min chronoamperometric step.

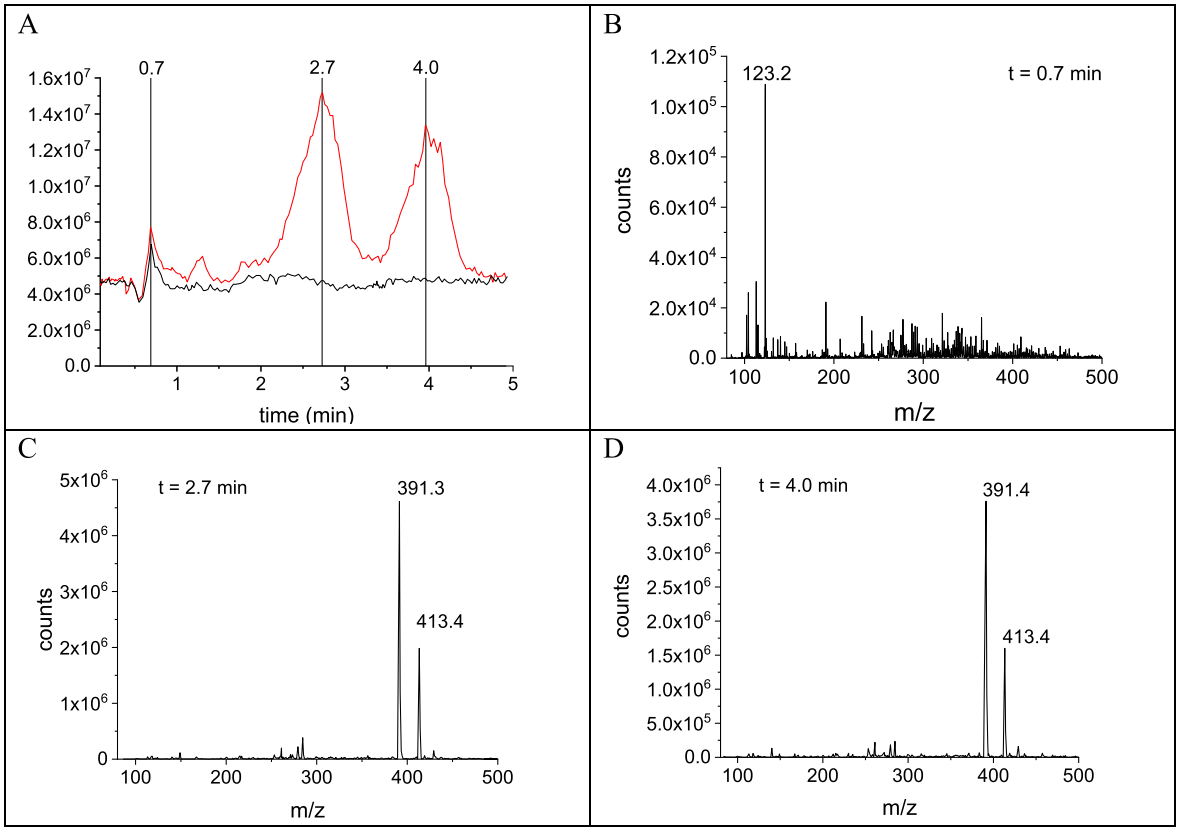

Fig. 6. **A**) TIC (total ion current) chromatogram: 20-times diluted sample of an aqueous solution of guaiacol 10 mM, TFA 20 mM and KCl 0.2 M. Black line (before), red line (after) 4 h constant potential electrolysis at +0.8 V. **B**) Mass spectrum of the species eluting at 0.7 min (guaiacol); **C**) Mass spectrum of the species eluting at 2.7 min **D**) Mass spectrum of the species eluting at 4.0 min.

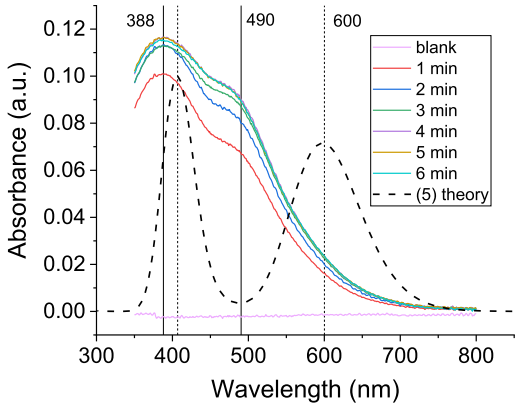

Fig. 7. UV–Vis spectra of an aqueous solution of guaiacol 1 mM, TFA 2 mM and KCl 0.1 M recorded at the beginning (blank, pink line) and after each minute of CA experiment. The dashed line represents the calculated spectra of (**5**). (For interpretation of the references to color in this figure legend, the reader is referred to the Web version of this article.)

2.4. LC-DAD and LC-MS

Products of guaiacol oxidation were separated via liquid chromatography and characterized by comparing theoretical UV–Vis spectra of the expected oxidation products with the recorded experimental UV–Vis spectra. Separation and spectra acquisition were performed with a LC Agilent 1050 series equipped with a quaternary low pressure LC pump and a multi-channel Diode Array Detector: liquid chromatography-UVVisDiodeArray (LC-DAD). LC-DAD runs were performed on a 20-fold diluted sample of the electrolyzed solution of guaiacol *-see paragraph Electrochemical experiments-*. Retention time (r.t.) for unreacted guaiacol was confirmed by injecting an aqueous solution of guaiacol that was not electrolyzed. Separation was carried out on a reversed-phase column, Alltech™ C18, 5 μm particle size, 150 × 2.1 mm, using a binary gradient elution program: solvent A: 0.1 % H_3PO_4 in Milli-Q® deionized water and solvent B, MeCN. The elution linear gradient was set as follows: 20 % B 1 min, 95 % B 20 min, 95 % B 5 min, 20 % B 2 min, 20 % B 6 min for a total gradient program duration of 34 min. Solvents were thoroughly degassed before elution. Sample was injected by a manual Rheodyne valve, 7725i model, with a 10 μL fixed loop. The LC column was kept at ambient temperature with an eluent flow of 0.3 mL/min. Diode-array detection was set to collect spectral data in the range of 220–500 nm. Single chromatograms were recorded at 275 nm, 385 nm and 495 nm. The Agilent Chemstation, LC rev. A, software was used for the system setup and signal acquisition. Characterization of electrolysis products was carried out via liquid chromatography-mass spectrometry (LC-MS) using a micro-LC Agilent 1200 series equipped with an ESI interface and an ion trap mass analyser, Agilent 6310A model. A reversed-phase column, ZORBAX® SB C18, 3.5 μm particle size, 30 × 2.1 mm, was used. The separation was carried out in isocratic elution mode with 20 % A (0.1 % Formic Acid, 10 mM Ammonium Acetate in Milli-Q® deionized water) and 80 % B (MeCN) mobile phase. The injection volume was set to 20 μL with a mobile phase flow of 0,2 mL/min. The temperature of the nitrogen stream for de-solvation was set to 350 °C. The mass analyser was set to scan a range of *m/z* from 80 to 500 amu. Both positive and negative potentials applied to the ESI interface were investigated, but ionization only occurred at positive potentials.

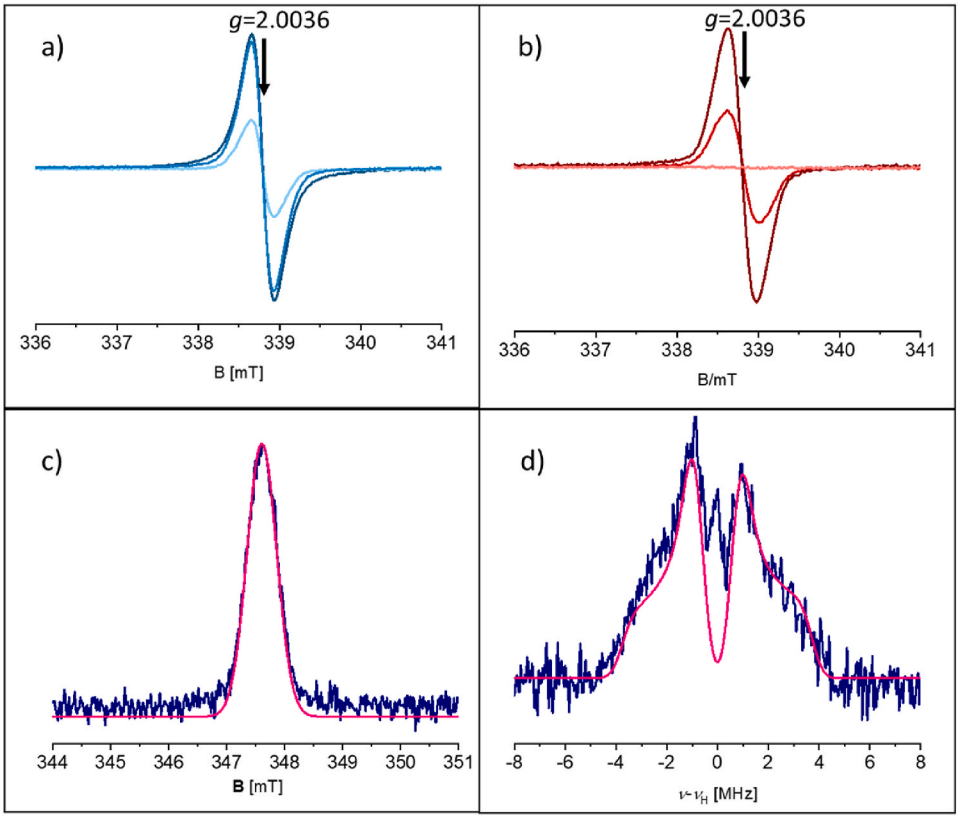

Fig. 8. a) Room-temperature CW-EPR spectra of a 50 % guaicol solution in 60 % $HClO_4$ at different time intervals (0, 30 min, 3 h); b) Room-temperature CW-EPR spectra recorded at different time intervals (0, 30 min, 3 h) of bulk electrolysis of a solution of guaiacol (52 % guaiacol: 45 % TFA: 3 % TBATFB by weight) subjected to *in-situ* bulk electrolysis at a constant potential of +0.8 V, Pt wires as both the WE and CE; c) Pulsed EPR spectrum of the electrolized guaiacol solution recorded at 10 K; d) ^{1}H Davies ENDOR spectrum of the electrolized guaiacol solution. The spectrum was recorded at a magnetic field corresponding to the maximum echo intensity (Fig. 8c) at 10 K. The frequency scale on the *x*-axis reports the deviation of the resonance lines from the ^{1}H Larmor frequency, ν_H.

Table 1
Spin Hamiltonian parameters derived from the simulation of EPR and ENDOR experiments. All hyperfine values in MHz.

g_{iso}	$A_{\|\|}$	$A_{\perp}$	a_{iso}	T
2.0036	7.5	1.5	3.5	2

2.5. EPR

In-situ EPR electrochemistry spectra were recorded at 295 K on a Bruker EMX X-band spectrometer equipped with a Bruker SHQ resonator and a PalmSens4™ potentiostat equipped with two Pt wires as both working and counter electrode. Two sample solutions were prepared with 1) 52 % of guaiacol, 45 % TFA and 3 % TBAHFP by weight and 2) 50 % by weight of both guaiacol and 60 % $HClO_4$. The spectra were simulated using EasySpin [19]. Pulsed-EPR spectra were recorded on a Bruker Elexys E580 spectrometer equipped with a dielectric ring resonator (ER 4118X-MD4) housed in a Cryogenic Cryogen-free variable temperature cryostat. During the measurements, the resonator was over-coupled to minimize ringdown following the application of the microwave pulses. The electron spin echo (ESE)-detected EPR spectra were measured at $T = 10$ K using a Hahn echo sequence ($\pi/2 - \tau - \pi - \tau -$ echo) while sweeping the field with $\tau = 200$ ns. X-band electron nuclear double resonance (ENDOR) measurements were carried out at 10 K by employing the Davies pulse sequence ($\pi - RF - \pi/2 - \tau - \pi - \tau - echo$) with $t_\pi = 200$ ns and $t_{RF} = 14000$ ns [20].

2.6. NMR

^{1}H NMR spectra were recorded with a Bruker FT-NMR AV-Neo 400 spectrometer operating at 400 MHz. Chemical shifts are reported in ppm compared to the signal of $CDCl_3$ (7.26 ppm). MestReNova 14.2.1–27684 software was used to process and analyse spectra. Samples for ^{1}H NMR analysis were prepared as follows: the electro-oxidized solution of guaiacol was first neutralized with a saturated $NaHCO_3$ solution, then transferred into a separatory funnel where the products were extracted with DCM (3 x 4 mL). The combined organic phases were then washed with brine and trace water was removed by drying over $MgSO_4$. The salt was removed by filtration over silica and the sample was concentrated by rotary evaporation. A drop of concentrated sample was then diluted in an NMR tube with 400 μL of $CDCl_3$.

2.7. Calculation details

All the theoretical results reported herein were performed in the framework of ab initio quantum mechanical based methods. For each species all possible oxidation states and spin multiplicity were considered. Unless stated otherwise, calculations were performed using C1 symmetry and unrestricted wave function with GAMESS [21] and Firefly Rev 8.20 [22] programs (Firefly is partially based on the GAMESS (US)8 source code). For each structure reported as stationary state shown in the PES versus reaction coordinates plot, reaction paths A, B, C, and D, molecular geometries were obtained by full optimization carried out at the B3LYP/6-31+G* level of the theory. To account for solute−solvent interaction, geometry optimization was carried out by using the Barone and Cossi's polarizable conductor model (CPCM) [23,24]; the latter is based on Tomasi's Polarized Continuum Model (PCM) [25]. The

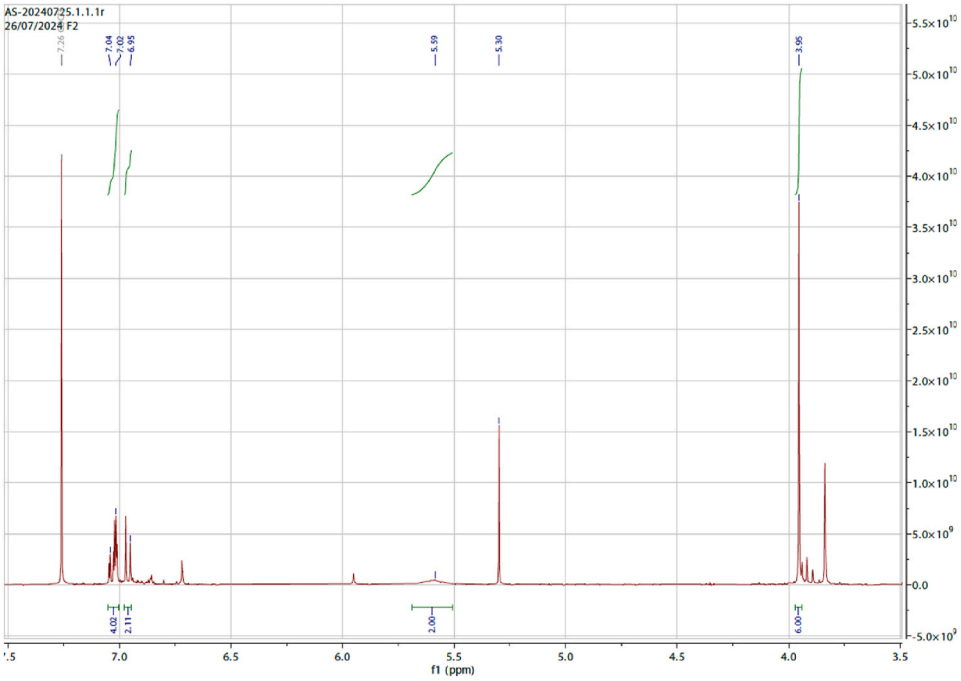

Fig. 9. **^{1}H NMR (400 MHz, $CDCl_3$) δ (ppm):** 7.04 (dd, 2H, $J_1 = 2$ Hz, $J_2 = 8$ Hz, Ar–*H*), 7.02 (d, 2H, $J = 2$, Ar–*H*), 6.95 (d, 2H, $J = 8$, Ar–*H*), 5.59 (s, 2H, Ar-O*H*), 3.95 (s, 6H, ArOCH_3). Solvent peaks: 7.26 ppm (s, CDCl3) and 5.30 ppm (s, residual DCM).

stability of all the species was checked by Hessian calculation.

3. Results and discussion

3.1. Electrochemical evidence

3.1.1. Cyclic voltammetry measurements

Fig. 1 shows the cyclic voltammetry (CV) curves of an aqueous solution of guaiacol (0.5 mM) in 1 mM TFA and 10 mM KCl. The potential was scanned in the range from − 0.2 to +1.2 V, starting from +0.4 V (which is the open circuit potential, OCP), at a scan rate of 0.1 V/s using GC as the working electrode.

The current measured in the first reduction forward scan (blue line) i.e. from +0.4 to −0.2 V is extremely low (about 50 μA). Then, in the following first oxidation scan (black line) i.e. from −0.2 V to +1.2 V, a minor peak is present at about +0.45 V, which is followed by a prominent one around +0.83 V. The oxidation reaction underlying the presence of the current peak at +0.83 V is the oxidation of guaiacol, which is in good agreement with previous studies [12]. Then, in the backward scan from +1.2 V to −0.2 V (orange line) the presence of a "new" major current peak centered at +0.2 V is noted. The latter is not present in the first reduction scan, so it is due to the reduction of species formed during the former oxidation cycle. The same applies for the oxidation peak at +0.54 V which dramatically increases after the first forward scan in the oxidation regime. This current peak assignation will be developed further on and confirmed by CV measurements at different potential scan windows, *vide infra* and in the Supporting Information (Fig. S1). Upon cycling, the oxidation peak at +0.83 V decreases in intensity and shifts towards less positive potentials, namely +0.75 V, while the oxidation peak at +0.54 V shifts in the opposite direction. This is possibly due to two different and competitive processes 1) to a decreasing efficiency in the guaiacol diffusion from the solution (polarization concentration); 2) the fouling of the electrode surface due to the start in the deposition of guaiacol oligomers, that screens it from the solution. The polymer is formed during the oxidation process and is not soluble in water, therefore it sticks to the electrode. During the CV measurements the solution turns into a brownish red color. The same behavior is observed during electrolysis experiments. Once the electrochemical potential is switched off, the color slowly reverts to pale pink-yellow, and over time a dark brown solid precipitate. This suggests that the oxidation product is a brown finely dispersed solid that settles slowly, or a possible equilibrium between two forms in solution, a coloured one and a colorless one. In the latter hypothesis, one of the species involved in the equilibrium might be insoluble, so it forms slowly then precipitate. The same coloration did not occur in the narrow-range CV measurement (see Supporting Information, Fig. S1) nor in a 30 min chronoamperometry at + 0.60 V (not shown). Moreover, hydrogen gas evolution from the CE is observed only upon reaching a +0.80 V potential. This confirms that guaiacol's oxidation is the main process taking place at +0.83 V.

3.1.2. Bulk electrolysis (chronoamperometry)

Fig. 2 shows a typical *i* vs t curve of a long-term (4 h) chronoamperometry (CA) experiment of a 10 mM guaiacol aqueous solution in 20 mM TFA and 0.2 M KCl base electrolyte. The CA is run at a constant oxidation potential of +0.8 V. The latter is selected according to the CV results shown in Fig. 1.

The CA oxidation current follows a monotonically decrease as a function of time. Indeed, the analysis of the CV curves, recorded as a function of the potential scan rate, shows that the electrochemical reaction underlying the presence of the +0.8 V main oxidation peak is diffusion limited (see Supporting Information, Fig. S2 and Fig. S3). The current passing between the electrodes reaches a plateau after about 60 min. After 4 h of CA, a deposit is observed on the WE surface, which eventually lead to the passivation of the electrode. This explains the decrease in current observed in the CVs shown in Fig. 1.

3.1.3. HER volume harvesting

Fig. 3 shows the volume of hydrogen produced at the CE (4 cm of Pt wire immersed in the solution, diameter = 0.50 mm) during electrolysis of guaiacol at +0.8 V: HER at the cathode and simultaneous sacrificial oxidation of guaiacol at the anode. Hydrogen evolution is faster and almost linear with time during the first hour.

This is due to progressive passivation of the anode caused by

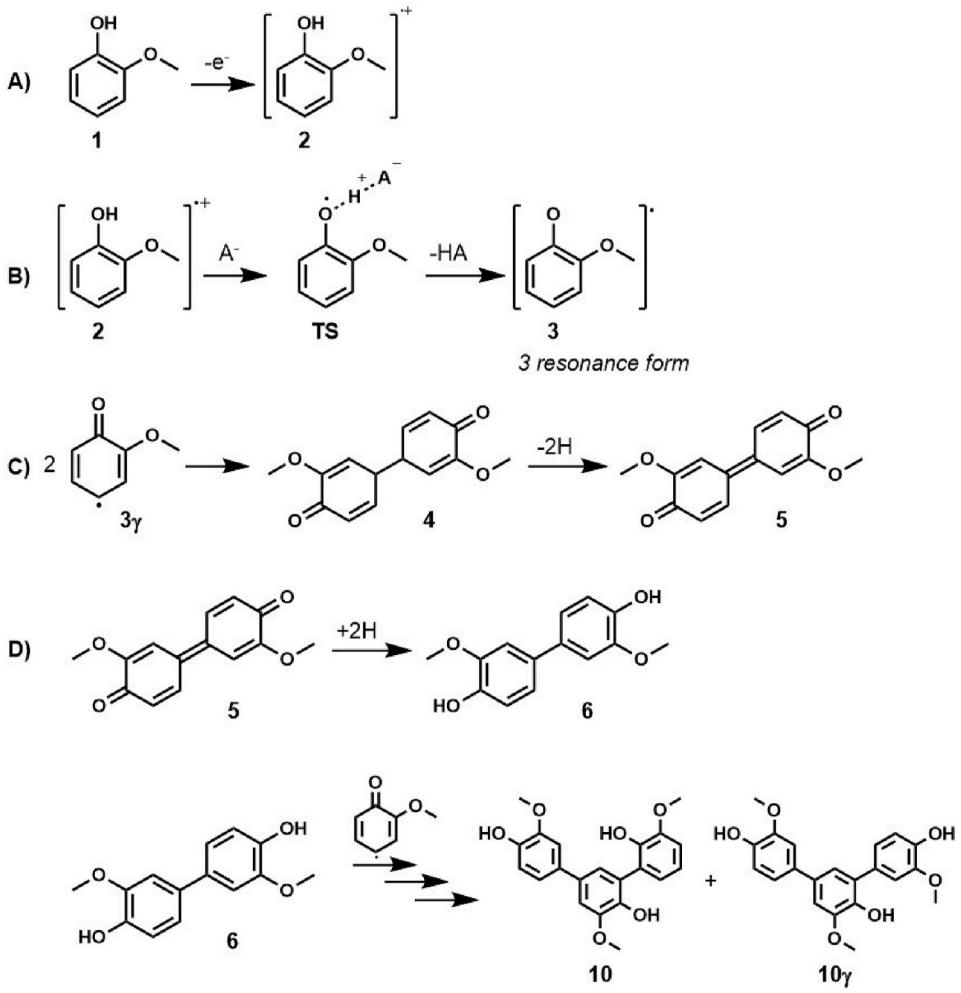

Scheme 1. Mechanism for the formation of guaiacol trimers, starting from electro-oxidation of guaiacol.

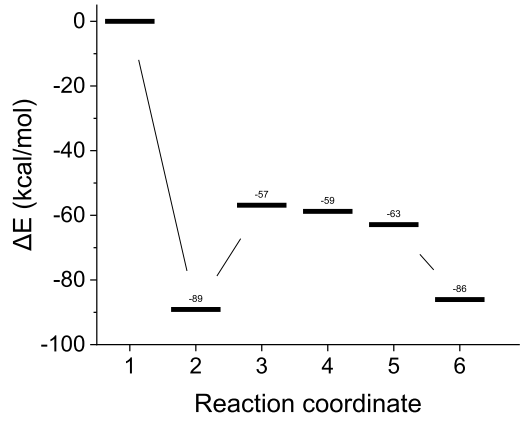

Fig. 10. Potential Energy Surface (PES) versus reaction coordinates plot of the species illustrated in Scheme 1. Calculations are performed with gaussian 16 at the UB3LYP/6-31+G* level of the theory. Geometry optimization was carried out by using the Barone and Cossi polarizable conductor model (CPCM).

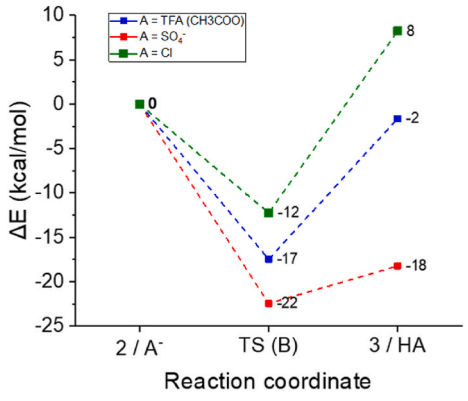

Fig. 11. Comparison in energy of different anions considered in step B of Scheme 1. Additional details concerning the guaiacol oxidation molecular mechanism are reported in Section 4 of the Supporting Information.

formation and deposit of insoluble guaiacol oligomers on the electrode's surface (*vide supra*). This drawback could be easily corrected by simple continuous mechanical cleaning and collection of the guaiacol oxidation products. From the volume of hydrogen evolved we estimated a Faradaic Efficiency (FE) of 75.5 % for the process of hydrogen evolution, calculation details are reported in the Supporting Information.

3.2. LC-DAD and LC-MS chromatography

Products formed during electrochemical oxidation of guaiacol were analysed using liquid chromatography-UVVisDiodeArray (LC-DAD) and liquid chromatography-mass (LC-MS) chromatography, with the aim to characterize the composition of the chemical products formed upon oxidation. Fig. 4 A (dashed line), shows a single peak in the

chromatogram at about 5.35 min that is guaiacol: the corresponding UV–vis spectrum (reported in the Supporting Information, Fig. S4) shows an absorption peak at 275 nm, in agreement with the theoretical spectrum of guaiacol and with spectra reported in the literature [26].

In the LC-DAD chromatogram of the electrolyzed solution (Fig. 4B, solid line), the peak of guaiacol is slightly shifted by 0.4 min. We exclude it is another reaction product because the UV–Vis spectrum associated with the peak is superimposable to that of guaiacol (see Supporting Information, Fig. S4). Moreover, some low-intensity peaks are present, meaning that various species are produced upon electrolysis. Notably, two coloured species have formed, having elution times of 2.49 min and 3.45 min. The first one absorbs at 385 and 495 nm (Fig. 4C and D), the latter absorbs only at 385 nm (Fig. 4C). The latter two species are more hydrophilic than guaiacol, thus retained for a shorter time. Remarkably, the UV spectrum of the species eluting at 3.944 min (Fig. 5) is superimposable to one reported in literature for the reduced form of a guaiacol dimer (i.e., 3,3′-dimethoxy-4,4′-dihydroxybiphenyl) [27].

To gain additional data about the structure of the oxidation products, we analysed the electrolyzed solution, as well as the guaiacol standard solution, using LC-MS chromatography. Fig. 6 shows LC-MS results, two species are eluted at retention times of 2.7 and 4.0 min (Fig. 6A).

These times do not correspond to any peak observed in the LC-DAD analysis since the chromatographic conditions were different. Interestingly, the mass spectra of both chromatographic peaks show the same *m/z* signal of 391 and 413 (Fig. 6C and D). The first one could be an ionized open-chain trimer bound to a sodium cation; the second one might be the sodium salt of the same trimer (see Supporting Information, Figs. S5 and S6, showing the experimental spectra and the possible relevant ion structures). It is possible that two isomers have formed, having slightly different polarities therefore eluting at different retention times. Remarkably, the pristine solution of non-electrolyzed guaiacol is ionized to a less extent (Fig. 6B), showing only a small peak at 0.7 min having a MS signal of 123, which might be guaiacol that lost a hydride anion in the ESI oxidation process. The same species (unreacted guaiacol) is also present in the electrolysed sample.

3.3. UV–vis spectroelectrochemistry

Fig. 7 sets out the dependence of product formation on oxidation time. The electrolysis was performed *in-situ* in a quartz cuvette, at +0.8 V, using a graphite lead as the WE, a Pt wire as the CE and a Ag/AgCl/KCl_{sat} as the RE. As can be seen in Fig. 7 (red line) after the first minute a coloured product has formed.

The oxidized species absorb in the range 350–650 nm, showing a maximum at 388 nm and a shoulder at around 490 nm. The intensity of the absorption band increased after each 1-min chronoamperometric step, until it reached a plateau after 4 min. Further oxidation steps did not lead to an increase in the absorbance of the solution. The absorption maxima wavelength and the overall shape of the UV–Vis spectrum of the electrolysed solution is in good agreement with data reported in literature for the enzymatic oxidation of guaiacol [27,28]. Main spectral pattern is attributed to the presence of 3,3′-dimethoxy-4,4′-biphenoquinone (**5**), which is unstable and spontaneously reduces to 3,3′-dimethoxy-4,4′-dihydroxybiphenyl (**6**).

3.4. EPR results

CW-EPR experiments were performed upon oxidation of a guaiacol solution with 60 % $HClO_4$ (50 % by weight of both guaiacol and hydrochloric acid solution). Immediately after mixing the solution turned blue and after a few minutes the reaction mixture reached a deep blue colour. EPR spectra were recorded at different time intervals after mixing and showed a single isotropic resonance centered at $g = 2.0036$, which is typical for carbon centered radicals (Fig. 8a). EPR measurements were also conducted on a pure guaiacol sample subjected to *in-situ* bulk electrolysis. The *in-situ* electrochemical EPR spectrum was recorded at different time intervals under a constant applied potential of +0.8 V using two Pt wires as both the WE and the CE. The spectrum grows in intensity as a function of time and is characterized by the same *g* factor observed in the case of the chemically oxidized system (Fig. 8b), suggesting that the same species is formed. Since the CW-EPR spectra show an unstructured line, Pulsed-EPR and ENDOR (Electron Nuclear DOuble Resonance) experiments have been carried out in order to obtain more details on the structure of the formed radical. The ^{1}H Davies ENDOR spectrum recorded at 10 K at a magnetic field position corresponding to the maximum of the echo (Fig. 8c) is shown in Fig. 8d, which shows a single, well-resolved axial hyperfine pattern with maximum coupling of 7.5 MHz. The full hyperfine tensor, as determined by spectral simulation, is reported in Table 1. Decomposition of the hyperfine tensor in the isotropic and anisotropic components provides an isotropic (a_{iso}) and dipolar (T) hyperfine coupling of 3.5 MHz and 2 MHz, respectively.

Based on the magnetic point-dipole approximation, the average distance of the order of 0.34 nm is estimated between the unpaired electron and the ^{1}H spins. The detection of a single hyperfine coupling implies that the ^{1}H nuclei present within the molecular scaffold of the radical species are all magnetically equivalent.

3.4.1. ^{1}H NMR characterization

Fig. 9 shows the ^{1}H NMR spectrum of the product of guaiacol electro-oxidation extracted from the reaction mixture.

A singlet of area 6 (at 3.95 ppm) implies the presence of two methoxy groups and a broad band of area 2 (at 5.59 ppm) is due to the presence of two hydroxyl groups. As for the 6 aromatic protons: 2 of them (the doublet at 6.95 ppm) have a coupling constant that is coherent with a meta-coupling ($J = 8$ Hz), 2 (the doublet at 7.02 ppm) have a coupling constant that is coherent with an ortho-coupling ($J = 2$ Hz), the third signal, the doublet of doublets at 7.04 ppm, couples with both ($J_1 = 2$ Hz, $J_2 = 8$ Hz). Considering 3 protons per ring, and the fact that substituents of guaiacol are in ortho, two of the ring protons are adjacent, the third is separated by one position: the carbon atom bearing the C–C bridge between the two rings. Chemical shifts and multiplicity splitting pattern confirm the symmetry the para-coupled dimer of guaiacol: 3,3′-dimethoxy-4,4′-dihydroxybiphenyl (**6**). These NMR data are in good agreement with those reported by Hwang et al. where the enzymatic guaiacol oxidation was studied [28].

3.5. Oxidation mechanism

Scheme 1 shows the single elementary steps considered in the polymerization of guaiacol. The elementary steps are inspired by the Kane−Maguire mechanism [13,14]. The overall scheme is similar to the one reported by Hwang et al. for the enzymatic oxidation of guaiacol [28]. Four different reaction paths are considered. Path A is the simple one-electron oxidation of guaiacol (**1**) leading to the relevant radical cation (**2**); in principle this is a reversible step. Suitable experimental conditions such as low temperature, very fast potential scan in cyclic voltammetry (CV), ultradry and oxygen free solvent, could allow to record a reversible or quasi-reversible voltammogram. Path B is a possible route for the coupling reaction, leading to the neutral radical species (**3**) by the dissociation of the hydroxylic O–H proton. (**3**) is a crucial reactive species in the supposed radical C–C coupling mechanism. Remarkably, a proton dissociation reaction is the key step. We will address explicitly the role of A^- in Fig. 10 [29]. The simplest follow-up reaction (path C) involves two radicals (**3**γ) and yields a stable closed-shell dimer, (**5**), via intermediate (**4**). Path D final product is the closed-shell dimer (**6**). An additional pathway that allows the formation of the peroxide might take place, but since it was studied in a previous work [18] and is highly reactive we did not focus on it. The formation of the trimer follows the same steps described before: starting from the dimer (**6**) it forms the radical cation (**7**, see Scheme S1), then it loses one hydrogen atom yielding the neutral radical (**8**, see Scheme S1)), which can combine with another monomer radical (**3**) to form the trimer (**10**).

Ionization energies were calculated for the monomer (**1**), the dimer (**4**) and the trimer (**9**, see Scheme S1) using the B3LYP-631+G(d) functional. Results suggest that the dimer is the first to be oxidized (with an IP of 7.049 eV) then the trimer (7.074 eV) and the monomer comes last (7.79 eV). This indicates that the production of the trimer is favoured. In Fig. 10 we show the calculated potential energy pattern of the principal components of the mechanism proposed in Scheme 1.

The overall process is downhill in energy if we consider the biphenyl species **6** as the final product, contrary to what was proposed (**5**) by Papouchado et al. [12]. Proton dissociation from **2** to the neutral radical **3** is uphill in energy, so we consider it to be nonspontaneous. Inclusion of explicit solvation effect contribution (continuum solvation water cpcm model) lowers the dissociation energy of **1** by 32 kcal/mol, with a relaxed scan, which is an energy barrier too high to allow a spontaneous proton dissociation (at 298 K). A completely different picture is obtained when the electrolyte anion (A^-) is considered. Fig. 11 shows the relaxed-scan PES concerning the proton dissociation assisted by three different anions: trifluoroacetate, sulphate and chloride anions. The elementary reaction considered is $\mathbf{2} + A^- \rightarrow \mathbf{3} + HA$. The overall process is downhill in energy with CF_3COO^- and HSO_4^-, and slightly uphill with Cl^-. In all three cases the intermediate is more stable than the products, by 20, 15 and 4 cal/mol respectively, which are energy differences low enough to allow the formation of the neutral radical **3**. Once formed, **3** exists in three resonance forms, all of which can couple forming the dimer. We focused our study on **3γ** homocoupling, that yields the para-para dimer.

4. Conclusions

An efficient Hydrogen evolution is observed during the electrolysis of acid solution of guaiacol (sacrificial reagent) in water. HER coupled with the guaiacol electrochemical oxidation was characterised in depth comparing both experimental results (CVs, chromatography, UV–Vis, EPR, ^{1}H NMR) with theoretical modelling. Remarkably, HER of the acidic guaiacol aqueous solution takes place at a much lower voltages, with respect to conventional water splitting, while maintaining a 75.5 % Faradaic efficiency. The amount of hydrogen production is a linear function of time for the first hour of electrolysis, as substantiated by kinetic measurements (volume of evolved hydrogen *vs.* time).

In a nutshell, the electrolysis of the acidic guaiacol aqueous solution is characterized by four main benefits.

1. a substantial decrease of the potential difference for the HER, 0.85 V with guaiacol vs. the minimum thermodynamic 1.23 V potential difference needed when coupling the HER with the sluggish OER in the water electrolysis.
2. HER is accompanied by the production of industrially appealing guaiacol-oligomers, contributing further to decreasing the cost of hydrogen production. It must be noted from the industrial/economic point of view that oligo-guaiacol derivatives exhibit significant reduced toxicity with respect to polyphenols, i.e. they are more sustainable fine chemical intermediates, while maintaining desirable technological properties in the large-scale production of plastics and resins [[30–34]].
3. As it is well known the main contribution to the overpotential in water electrolysis is due to the OER sluggish process, and catalysers are needed to improve efficiency [5–9,35], see also for instance Chapter 16 in Ref. [36]. Whilst guaiacol oxidation runs efficiently on not-precious carbon-based surfaces like graphite and glassy carbon.
4. Finally, due to the completely different chemistry, there is not any hydrogen peroxide formation.

CRediT authorship contribution statement

Andrea Severini: Methodology, Investigation, Data curation, Conceptualization. **Camilla Ferrari:** Methodology, Investigation, Formal analysis, Data curation. **Andrea Marchetti:** Writing – original draft, Methodology, Investigation, Formal analysis, Data curation, Conceptualization. **Francesco Vizza:** Writing – review & editing, Validation, Resources, Project administration. **Marco Bonechi:** Visualization, Software, Data curation. **Massimo Innocenti:** Writing – original draft, Visualization, Resources, Project administration, Methodology, Funding acquisition. **Valeria Lagostina:** Methodology, Investigation, Formal analysis, Data curation. **Enrico Salvadori:** Writing – review & editing, Methodology, Investigation, Formal analysis, Data curation. **Mario Chiesa:** Writing – review & editing, Methodology, Investigation, Formal analysis, Data curation. **Fabrizio Roncaglia:** Writing – review & editing, Methodology, Investigation, Formal analysis, Data curation, Conceptualization. **Claudio Fontanesi:** Writing – review & editing, Writing – original draft, Methodology, Investigation, Conceptualization.

Declaration of competing interest

The authors declare that they have no known competing financial interests or personal relationships that could have appeared to influence the work reported in this paper.

Acknowledgements

This work was supported by the Italian MUR through the PRIN 2022 Project “FUTURO 2022NW4P2T” funded by National Recovery and Resilience Plan (PNRR), Italy, Mission 04 Component 2 Investment 1.1 – NextGenerationEU (CUP: E53D23008490006). "From metal nanoparticles to molecular complexes in electrocatalysis for green hydrogen evolution and simultaneous fine chemicals production (FUTURO)”, PI Prof. Massimo Innocenti. Then, from Fondazione di Modena, Fondo di Ateneo per la Ricerca Anno 2023, linea FOMO, Progetto AMNESIA, PI Claudio Fontanesi. Financial support is also gratefully acknowledged from Consorzio Interuniversitario Nazionale per la Scienza e Tecnologia dei Materiali (INSTM), fondi triennali: “INSTM21MOFONTANESI”. Authors acknowledge also financial support by Fondazione CR Firenze: Fondazione per la Ricerca e l’Innovazione dell’Università degli Studi di Firenze and Confindustria Firenze: FABER4 project framework.

Appendix A. Supplementary data

Supplementary data to this article can be found online at https://doi.org/10.1016/j.ijhydene.2025.03.439.

References

[1] Beswick RR, Oliveira AM, Yan Y. Does the green hydrogen economy have a water problem? ACS Energy Lett 2021;6:3167–9. https://doi.org/10.1021/acsenergylett.1c01375.
[2] Li W, Tian H, Ma L, Wang Y, Liu X, Gao X. Low-temperature water electrolysis: fundamentals, progress, and new strategies. Mater Adv 2022;3:5598–644. https://doi.org/10.1039/D2MA00185C.
[3] Woods P, Bustamante H, Aguey-Zinsou K-F. The hydrogen economy - where is the water? Energy Nexus 2022;7:100123. https://doi.org/10.1016/j.nexus.2022.100123.
[4] Lohmann-Richters FP, Renz S, Lehnert W, Müller M, Carmo M. Review—challenges and opportunities for increased current density in alkaline electrolysis by increasing the operating temperature. J Electrochem Soc 2021;168:114501. https://doi.org/10.1149/1945-7111/ac34cc.
[5] Mtangi W, Kiran V, Fontanesi C, Naaman R. Role of the electron spin polarization in water splitting. J Phys Chem Lett 2015;6:4916–22. https://doi.org/10.1021/acs.jpclett.5b02419.
[6] Mtangi W, Tassinari F, Vankayala K, Vargas Jentzsch A, Adelizzi B, Palmans ARA, et al. Control of electrons’ spin eliminates hydrogen peroxide formation during water splitting. J Am Chem Soc 2017;139:2794–8. https://doi.org/10.1021/jacs.6b12971.
[7] Mondal PC, Mtangi W, Fontanesi C. Chiro-spintronics: spin-dependent electrochemistry and water splitting using chiral molecular films. Small Methods 2018;2:1700313. https://doi.org/10.1002/smtd.201700313.
[8] Gazzotti M, Stefani A, Bonechi M, Giurlani W, Innocenti M, Fontanesi C. Influence of chiral compounds on the oxygen evolution reaction (OER) in the water splitting process. Molecules 2020;25:3988. https://doi.org/10.3390/molecules25173988.

[9] Garcés-Pineda FA, Blasco-Ahicart M, Nieto-Castro D, López N, Galán-Mascarós JR. Direct magnetic enhancement of electrocatalytic water oxidation in alkaline media. Nat Energy 2019;4:519–25. https://doi.org/10.1038/s41560-019-0404-4.
[10] Shen X, Meng Q, Mei Q, Liu H, Yan J, Song J, et al. Selective catalytic transformation of lignin with guaiacol as the only liquid product. Chem Sci 2020; 11:1347–52. https://doi.org/10.1039/C9SC05892C.
[11] Martău GA, Călinoiu L-F, Vodnar DC. Bio-vanillin: towards a sustainable industrial production. Trends Food Sci Technol 2021;109:579–92. https://doi.org/10.1016/j.tifs.2021.01.059.
[12] Papouchado L, Bacon J, Adams RN. Potential step cyclic voltammetry for the study of electrode reaction mechanisms. J Electroanal Chem Interfacial Electrochem 1970;24:A1–5. https://doi.org/10.1016/S0022-0728(70)80029-8.
[13] Wallace GG, Teasdale PR, Spinks GM, Kane-Maguire LAP. Conductive electroactive Polymers: Intelligent Polymer Systems. third ed. third ed. Boca Raton: CRC Press; 2008. https://doi.org/10.1201/9781420067156.
[14] Kane-Maguire LAP, Wallace GG. Chiral conducting polymers. Chem Soc Rev 2010; 39:2545–76. https://doi.org/10.1039/b908001p.
[15] Bruno C, Benassi R, Passalacqua A, Paolucci F, Fontanesi C, Marcaccio M, et al. Electrochemical and theoretical investigation of corannulene reduction processes. J Phys Chem B 2009;113:1954–62. https://doi.org/10.1021/jp8045092.
[16] Bruno C, Paolucci F, Marcaccio M, Benassi R, Fontanesi C, Mucci A, et al. Experimental and theoretical study of the p- and n-doped states of alkylsulfanyl octithiophenes. J Phys Chem B 2010;114:8585–92. https://doi.org/10.1021/jp9122612.
[17] Choudhury S, Tu Z, Nijamudheen A, Zachman MJ, Stalin S, Deng Y, et al. Stabilizing polymer electrolytes in high-voltage lithium batteries. Nat Commun 2019;10:3091. https://doi.org/10.1038/s41467-019-11015-0.
[18] Bonechi M, Innocenti M, Vanossi D, Fontanesi C. The fundamental and underrated role of the base electrolyte in the polymerization mechanism. The resorcinol case study. J Phys Chem A 2021;125:34–42. https://doi.org/10.1021/acs.jpca.0c07702.
[19] Stoll S, Schweiger A. EasySpin, a comprehensive software package for spectral simulation and analysis in EPR. J Magn Reson 2006;178:42–55. https://doi.org/10.1016/j.jmr.2005.08.013.
[20] Davies ER. A new pulse endor technique. Phys Lett 1974;47:1–2. https://doi.org/10.1016/0375-9601(74)90078-4.
[21] Schmidt MW, Baldridge KK, Boatz JA, Elbert ST, Gordon MS, Jensen JH, et al. General atomic and molecular electronic structure system. J Comput Chem 1993; 14:1347–63. https://doi.org/10.1002/jcc.540141112.
[22] Granovsky AA. Firefly version 8.0.0. http://classic.chem.msu.su/gran/firefly/index.html; 2016.
[23] Bliznyuk V, Möhwald H. Miscibility of cyanine dyes in two-dimensional aggregates. Thin Solid Films 1995;261:275–9. https://doi.org/10.1016/S0040-6090(94)06499-7.
[24] Barone V, Cossi M. Quantum calculation of molecular energies and energy gradients in solution by a conductor solvent model. J Phys Chem A 1998;102: 1995–2001. https://doi.org/10.1021/jp9716997.
[25] Miertuš S, Scrocco E, Tomasi J. Electrostatic interaction of a solute with a continuum. A direct utilizaion of AB initio molecular potentials for the prevision of solvent effects. Chem Phys 1981;55:117–29. https://doi.org/10.1016/0301-0104(81)85090-2.
[26] Wang Y, Ding Z, Zhang Y, Wei C, Xie Z. Luffa pretreated by plasma oxidation and acidity to Be used as cellulose films. Polymers 2018;11:37. https://doi.org/10.3390/polym11010037.
[27] Doerge DR, Divi RL, Churchwell MI. Identification of the colored guaiacol oxidation product produced by peroxidases. Anal Biochem 1997;250:10–7. https://doi.org/10.1006/abio.1997.2191.
[28] Hwang S, Lee C-H, Ahn I-S. Product identification of guaiacol oxidation catalyzed by manganese peroxidase. J Ind Eng Chem 2008;14:487–92. https://doi.org/10.1016/j.jiec.2008.02.008.
[29] Choudhury S. Stabilizing polymer electrolytes in high-voltage lithium batteries. In: Choudhury S, editor. Rational Design of Nanostructured Polymer Electrolytes and Solid–Liquid Interphases for Lithium Batteries. Cham: Springer International Publishing; 2019. p. 199–227. https://doi.org/10.1007/978-3-030-28943-0_11.
[30] Cerfontain H, Coenjaarts NJ, Koeberg-Telder A. Sulfonation and sulfation on reaction of 1,2-dihydroxybenzene and its methyl ethers in concentrated aqueous sulfuric acid. Recl Trav Chim Pays-Bas 1988;107:325–30. https://doi.org/10.1002/recl.19881070405.
[31] Abdelaziz OY, Vives MB, Mankar SV, Warlin N, Nguyen TT, Zhang B, et al. Recent strides toward transforming lignin into plastics and aqueous electrolytes for flow batteries. iScience 2024;27. https://doi.org/10.1016/j.isci.2024.109418.
[32] Lemouzy S, Delavarde A, Lamaty F, Bantreil X, Pinaud J, Caillol S. Lignin-based bisguaiacol diisocyanate: a green route for the synthesis of biobased polyurethanes. Green Chem 2023;25:4833–9. https://doi.org/10.1039/D3GC00704A.
[33] Trullemans L, Koelewijn S-F, Boonen I, Cooreman E, Hendrickx T, Preegel G, et al. Renewable and safer bisphenol A substitutes enabled by selective zeolite alkylation. Nat Sustain 2023;6:1693–704.
[34] Periyasamy T, Asrafali SP, Muthusamy S, Kim S-C. Replacing bisphenol-A with bisguaiacol-F to synthesize polybenzoxazines for a pollution-free environment. New J Chem 2016;40:9313–9. https://doi.org/10.1039/C6NJ02242A.
[35] Zhao Y, Adiyeri Saseendran DP, Huang C, Triana CA, Marks WR, Chen H, et al. Oxygen Evolution/reduction reaction catalysts: from in situ monitoring and reaction mechanisms to rational design. Chem Rev 2023;123:6257–358. https://doi.org/10.1021/acs.chemrev.2c00515.
[36] Mohapatra S, Nguyen TA, Nguyen-Tri P, editors. Front-matter. Noble Metal-Metal Oxide Hybrid Nanoparticles. Woodhead Publishing; 2019. i–iii. https://doi.org/10.1016/B978-0-12-814134-2.00030-9.